Supplementary Materials for

Timing and Specificity of Cotranslational Nascent Protein Modification

Chien-I Yang, Hao-Hsuan Hsieh and Shu-ou Shan*

Division of Chemistry and Chemical Engineering, California Institute of Technology

1200 E. California Blvd, Pasadena, CA 91125

*Correspondence to: sshan@caltech.edu

This file includes:

Supplementary Methods

Figures S1–S9

Table S1

Supplementary References

www.pnas.org/cgi/doi/10.1073/pnas.1912264116

Supplemental Methods

Plasmid and strain construction

The expression vector pET28a was used for the cloning of PDF, MAP, MAP-H79A and MAP-HA. MAP-H79A contains a cleavable N-terminal $(His)_6$-SUMO tag and a C-terminal GLPATGG extension, which does not affect the activity of MAP. For *in vitro* transcription and translation of RNCs, DNA sequences coding the FtsQ or luciferase nascent chains were subcloned via Gibson cloning (*1*) into pUC19 containing T7 promoter and the ribosome-binding site (*2*, *3*). The *Ms*-sup1 stalling sequence was fused to the C-termini of nascent chain sequences via Fastcloning (*4*). For the cotranslational NME assay, DNA fragments coding thioredoxin-fusion proteins were cloned into the pK7 plasmid (*5*) between the T7 promoter and T7 terminator using Gibson cloning. To construct the strain harboring C-terminal HA tagged MAP for preparation of S30 extract, the genomic MAP in KC6 (A19 *ΔendA met+ ΔtonA ΔspeA ΔtnaA ΔsdaA ΔsdaB ΔgshA*;(*6*)) was modified using λ-red recombination (*7*).

Protein expression and purification

PDF was purified as described (*8*). Briefly, BL21 star (DE3) cells (Invitrogen) at OD_{600} = 0.5 were induced with 0.5 mM IPTG at 30 °C for 4 h, and lysed by sonication in buffer A (50 mM Hepes-KOH and 20 mM $NiSO_4$, pH 7.5) containing ProBlock Gold protease inhibitor cocktail (GoldBio). Clarified lysate was dialyzed overnight against buffer A. After ultracentrifugation for 30 min at 55,000 rpm, 4 °C in a Ti 70 rotor (Beckmann Coulter), the supernatant was loaded onto MonoQ 10/100 GL (GE Healthcare) equilibrated with buffer B (50 mM Hepes-KOH, 10% glycerol and 5 mM $NiSO_4$, pH 7.5) and eluted with a linear gradient of 0–500 mM KCl. Fractions containing single PDF band were collected and dialyzed against buffer C (50 mM Hepes-KOH, 100 mM NaCl, and 0.2 mM $CoCl_2$, pH 7.5) before storage at –80 °C.

Wild-type MAP, MAP-K226E and MAP-HA were purified as described (*9*). BL21 star (DE3) cells at OD_{600} = 0.6 were induced with 0.5 mM IPTG at 30 °C for 3 h, and lysed by sonication in buffer D (50 mM Hepes-KOH, 10% glycerol and 0.2 mM $CoCl_2$, pH 7.5) containing protease inhibitor. Protein in clarified lysate was precipitated with 0–80% ammonium sulfate. The pellet was resuspended with buffer D, dialyzed overnight against buffer D, and loaded onto Q Sepharose Fast Flow column (GE Healthcare). For wild-type MAP and MAP-K226E, proteins were eluted with

buffer C and further purified with MonoQ 10/100 GL using a linear gradient of 0–200 mM NaCl. Purified proteins were supplemented with 20% glycerol before storage at –80 °C. MAP-HA was eluted from Q Sepharose with a linear gradient of 0–500 mM NaCl, and fractions containing purified proteins were supplemented with 20% glycerol and stored at –80 °C.

To express MAP-H79A, BL21 star (DE3) cells at OD_{600} = 0.6 were induced with 0.5 mM IPTG at 30 °C for 3 h, and lysed by sonication in buffer D containing protease inhibitor. Clarified cell lysates were loaded onto Ni-NTA equilibrated with buffer E (50 mM Hepes-KOH, 500 mM NaCl, 10% glycerol and 20 mM imidazole, pH 7.5). Proteins were eluted with buffer F (50 mM Hepes-KOH, 150 mM NaCl, 10% glycerol and 500 mM imidazole, pH 7.5), incubated with His_6-Ulp1protease and dialyzed overnight against buffer G (50 mM Hepes-KOH, 50 mM NaCl, 10% glycerol, pH 7.5). Tag-free proteins were passed through Ni-NTA, and further purified with MonoQ using a linear gradient of 0–200 mM NaCl. Purified proteins were supplied with 0.2 mM $CoCl_2$ and 20% glycerol before storage in –80 °C.

RNC purification

Radiolabeled RNCs were generated by *in vitro* translation in *E. coli* S30 extract supplemented with ^{35}S-Met as described previously (*10*). In brief, plasmids coding for nascent peptide sequence were transcribed and translated in 0.5 mL of mixture containing 12 mM magnesium glutamate, 10 mM ammonium glutamate, 175 mM potassium glutamate, 1.2 mM ATP, 0.86 mM each of GTP, CTP, and UTP, 34 μg/mL folinic acid, 0.17 mg/mL *E. coli* tRNA (Roche), 2 mM each of amino acids except methionine, 10 μM methionine, 0.44 μM ^{35}S-methionine, 33 mM phosphoenolpyrovate, 0.33 mM β-nicotinamide adenine dinucleotide, 0.26 mM CoA, 2.7 mM sodium oxalate, 1.5 mM spermidine, 1 mM putrescine, 4 μM anti-ssr1 oligonucleotide, 28% (vol/vol) S30 extract, 5 μM actinonin, and 2 μM T7 RNA polymerase, pH 7.8, at 30 °C for 1.5 h. The reaction was loaded onto a 40 mL sucrose gradient (10–50% sucrose in 50 mM Hepes-KOH, 500 mM KOAc, 100 mM $Mg(OAc)_2$, 0.1% Triton X-100, 1 μM actinonin and 1 mM TCEP, pH 7.5) and centrifuged for 15 h at 23,000 rpm, 4 °C in a SW32 Ti rotor (Beckmann Coulter). Monosome fractions were collected and centrifuged for 2 h at 100,000 rpm, 4 °C in a TLA 100.3 rotor (Beckmann Coulter). Pellets were washed and dissolved in assay buffer (50 mM Hepes-KOH, 150 mM KOAc, 10 mM $Mg(OAc)_2$, and 1 mM TCEP, pH 7.5), and stored at –80 °C. To prepare Cm-labeled RNCs, 75 μM Cm, 12 μM RF1 aptamer and 12 μM coumarine synthetase were included in the translation reaction,

methionine was increased to 2 mM, and ^{35}S-methionine was omitted. The nascent peptide concentrations were determined by scintillation counting or fluorescence measurement. For the RNC used in this study, 7–15% of the ribosomes contained the nascent peptide.

RNC NME assays

Methionine cleavage assay. Pre-steady state kinetic measurements were carried out under single-turnover condition using an RQF-3 Quench-flow instrument (KinTek). To remove the formyl group prior to measuring methionine cleavage, 20 nM RNC labeled with a single ^{35}S methionine at the N-terminus was incubated with PDF (100 nM) in assay buffer (50 mM Hepes-KOH, 150 mM KOAc, 10 mM $Mg(OAc)_2$, and 1 mM TCEP, pH 7.5) with 0.1 mM $CoCl_2$ at room temperature for at least 15 min. The reaction was initiated by rapidly mixing deformylated RNC with an equal volume of MAP solution at varying concentrations, and quenched with 10% TCA at specified time points. Quenched reactions were centrifuged at 18,000 g, 4 °C for 10 min to precipitate the proteins. The supernatant containing released ^{35}S-methionine was subjected to scintillation counting for quantification. The amount of free methionine was normalized against the total amount of nascent chain, and the data was fit to Eq. 1,

$$\frac{[Met]}{[RNC]_0} = C(1 - e^{-k_{obs}t}) \quad (1)$$

where k_{obs} is the observed rate constant, and C is the maximum fraction of RNC that can be processed.

Coupled deformylation assay. 20 nM RNC labeled with a single ^{35}S methionine at the N-terminus was rapidly mixed with an equal volume of enzyme solution containing 2 μM MAP and varying concentrations of PDF. The reaction was quenched with 10% TCA and quantified as described above.

ACT-quench deformylation assay. 20 nM RNC labeled with a single ^{35}S methionine at the N-terminus was mixed with varying concentrations of PDF to initiate the reaction. For substrates FtsQ-S2 and FtsQ-T2, the reaction was quenched with 40 μM of ACT at specified times, and the deformylated methionine on the nascent chain was released by incubation with 0.1 μM MAP for 10 s. For FtsQ-V2 and FtsQ-N2, 80 μM ACT was used to quench the reaction, followed by a 5

min incubation with 0.25 μM MAP. The reaction was quenched with 10% TCA and quantified as described above.

Kinetic analysis. To determine the kinetic parameters under single-turnover conditions, the following enzymatic reaction scheme was considered:

$$E + S \underset{k_{-1}}{\overset{k_1}{\rightleftharpoons}} E \bullet S \xrightarrow{k_2} E \bullet P$$

The expression for the observed rate constant of the reaction (k_{obsd}) at a given enzyme concentration was derived using the Cleland method (*11*):

$$k_{obsd} = \frac{k_2[E]}{\frac{k_{-1}+k_2}{k_1}+[E]} = \frac{k_{cat}[E]}{K_M+[E]} \quad (2)$$

where $k_{cat} = k_2$, $K_M = \frac{k_{-1}+k_2}{k_1}$, and $k_{cat}/K_m = \frac{k_1 k_2}{k_2+k_{-1}}$.

Under k_{cat}/K_m conditions, [E] → 0, which gives us:

$$k_{obsd} = \frac{k_1 k_2}{k_2+k_{-1}}[E] = k_{cat}/K_m[E] \quad (3)$$

k_{cat}/K_m was obtained from a linear fit of k_{obs} values against effective enzyme concentration (see next paragraph) at sub-saturating enzyme concentrations. We note that the expression for k_{cat}/K_m is the same, regardless of whether single or multiple turnover conditions are used.

To correct for the effect of enzyme depletion by vacant ribosomes (~50–100 nM) in the reactions, we calculated the concentration of ribosome-bound PDF and MAP concentrations (Table S1) using quadratic equations derived from the following equilibria

$$\begin{aligned} \text{ribosome} + \text{PDF} &\underset{}{\overset{K_d^{PDF}}{\rightleftharpoons}} \text{ribosome} \cdot \text{PDF} \\ \text{ribosome} + \text{MAP} &\underset{}{\overset{K_d^{MAP}}{\rightleftharpoons}} \text{ribosome} \cdot \text{MAP} \end{aligned} \quad (4)$$

in which the values of K_d^{PDF} and K_d^{MAP} were 1.8 μM and 2.4 μM, respectively, as reported previously (*12*, *13*). The effective enzyme concentration was calculated by subtracting ribosome-bound enzyme from total enzyme concentration.

MAP peptidase activity assay

The peptidase activity of purified MAP on a peptide substrate, Met-Gly-Met-Met, was measured by a coupled assay as described (*9*). Briefly, the N-terminal methionine released by MAP was oxidized by *L*-amino-acid oxidase and peroxidase, resulting in changes in absorbance at 440 nm. Each reaction (100 μL) contained 50 mM Hepes-KOH (pH 7.5), 0.2 mM $CoCl_2$, 0.1 mg/mL *o*-dianisidine (Sigma), 3 units of horseradish peroxidase (Sigma), 0.5 units of *L*-amino-acid oxidase (Sigma), 0.2 μM MAP and varying concentrations of Met-Gly-Met-Met (Genscript). The substrate concentration dependence of initial velocities was fit to the Michaelis-Menten equation to obtain the k_{cat} and K_m values.

Fluorescence labeling of MAP and MAP-H79A

MAP and MAP-H79A containing a C-terminal GLPATGG tag were labeled with BODIPY-FL (Invitrogen) at the C-termini using sortase-mediating reactions (*14*). The labeling reactions contained 50 μM MAP, 120 μM His_6-tagged sortase A and 250 μM GGGC-BODIPY peptide, and incubated at room temperature for 4 h. Sortase A was removed by incubation with Ni-NTA resin, and excess peptides were removed using Sephadex G25 (Sigma) gel filtration column. The labeling efficiency was estimated to be >90%.

Fluorescence measurement

All fluorescent measurements were carried out at room temperature in assay buffer containing 0.1 mM $CoCl_2$. Emission spectrum and equilibrium titrations were measured on a Fluorolog-3 spectrofluorometer (HORIBA) using an excitation wavelength of 360 nm. Cm-labeled RNC (8 nM) was deformylated with 100 nM PDF for at least 15 min and incubated with indicated proteins before the measurement. For equilibrium titrations, the fluorescent signals were normalized to the signal without MAP-H79A, and fit to Eq. 5,

$$F_{obsd} = F_{max} \cdot \frac{[RNC] + [MAP] + K_d - \sqrt{([RNC] + [MAP] + K_d)^2 - 4 \cdot [RNC] \cdot [MAP]}}{2 \cdot [RNC]} \quad (5)$$

in which [RNC] and [MAP] are input values as described, F_{obsd} is the normalized fluorescent signal, F_{max} is the signal at saturating MAP concentration, and K_d is the equilibrium dissociation constant of the RNC-MAP complex. The association rate constant (k_{on}) of the RNC-MAP complex was measured on a Kintek stopped-flow apparatus. Cm-labeled RNC (16 nM) was deformylated with

200 nM PDF for at least 15 min before the measurement, and mixed with an equal volume of various concentrations of MAP-H79A to initiate the reaction. The fluorescent signals (*I*) were monitored over time, and the time courses were fit to Eq. 6,

$$I(t) = I_0 + (I_{max} - I_0) \cdot \left(1 - e^{-k_{app}t}\right) \quad (6)$$

where I_0 is the signal at t = 0, I_{max} is the signal at t = ∞, and k_{app} is the observed rate constant for complex assembly. The values of k_{app} were plotted against [MAP-H79A] and fit to Eq. 7,

$$k_{app} = k_{on} \cdot [MAP] + k_{off} \quad (7)$$

where k_{on} and k_{off} are the association and dissociation rate constants for the RNC-MAP complex, respectively.

Cotranslational NME assay

PCR fragments encoding T7 promoter and FtsQ-X2-TrxA were transcribed and translated in 10 μL of mixture containing 12 mM magnesium glutamate, 10 mM ammonium glutamate, 175 mM potassium glutamate, 1.2 mM ATP, 0.86 mM each of GTP, CTP, and UTP, 34 μg/mL folinic acid, 0.17 mg/mL *E. coli* tRNA (Roche), 2 mM each of amino acids except methionine, 2% (v/v) ^{35}S-methionine, 33 mM phosphoenolpyrovate, 0.33 mM β-nicotinamide adenine dinucleotide, 0.26 mM CoA, 2.7 mM sodium oxalate, 1.5 mM spermidine, 1 mM putrescine, 4 μM anti-ssr1 oligonucleotide, 28% (v/v) S30 extract, 1 unit/μL RNase inhibitor (NEB) and 6 μM T7 RNA polymerase, pH 7.8, at 30 °C for 30 min. Where indicated, the control reactions contained 5 μM actinonin. Reactions were quenched with SDS sample loading buffer (60 mM Tris-HCl, 1.6% SDS, 30 mM EDTA, 2.6 M urea, 30 mM DTT, 15% glycerol, pH 6.8) and analyzed by SDS-PAGE and autoradiography.

Preparation of ribosome-free cell extracts

S30 extracts were supplemented with 500 mM KOAc and ultra-centrifuged in TLA120.2 (Beckman-Coulter) rotor at 100,000 rpm, 4 °C for 1 h to sediment the ribosomes. The supernatant

was dialyzed against buffer containing 10 mM Tris-HCl (pH 8.2), 150 mM KOAc, and 14 mM $Mg(OAc)_2$.

Western blots for protein quantification in cell extracts

The concentrations of purified proteins were determined by the absorption at 280 nm (Strep-Sbh1) or Bradford assay (PDF and MAP-HA). Rabbit anti-PDF (MBS2547699; MyBiosource), mouse anti-HA (Genscript), and mouse anti-Strep (Genscript) are commercially available. IRDye 800CW goat anti–rabbit IgG (925-32211; LI-COR Biosciences) or IRDye 800CW goat anti–mouse IgG (925-32210; LI-COR Biosciences) were used for detection, and the signals were quantified by the Odyssey CLx imaging system (LI-COR Biosciences).

Simulation modeling for cotranslational NME

A kinetic framework was constructed to describe the cotranslational NME of an *n*-residue nascent protein under single turnover conditions (Fig. 4A). This describes the reactions during *in vitro* translation in S30 lysate, in which the concentration of ribosome is in excess of actively translated nascent proteins (Fig. S6A). The scheme in Fig. 4A can be described by the following differential equations for every nascent chain length *i*, ranging from 1 to *n*:

$$\frac{d}{dt}fmRNC(i,t) = k_{trans} \cdot fmRNC(i-1,t) - k_{trans} \cdot fmRNC(i,t) - k_i^{PDF} \cdot fmRNC(i,t) \quad (8)$$

$$\frac{d}{dt}mRNC(i,t) = k_{trans} \cdot mRNC(i-1,t) - k_{trans} \cdot mRNC(i,t) + k_i^{PDF} \cdot fmRNC(i,t) - k_i^{MAP} \cdot mRNC(i,t) \quad (9)$$

$$\frac{d}{dt}RNC(i,t) = k_i^{MAP} \cdot mRNC(i,t) \quad (10)$$

where *fmRNC*, *mRNC* and *RNC* represent the concentrations of unprocessed, deformylated and demethionylated RNCs, respectively. Note that at the start of translation elongation (i =1), $fmRNC(i\text{-}1, t) = mRNC(i\text{-}1, t) = 0$. At translation termination ($i = n$), the terms $k_{trans} \cdot fmRNC(i, t)$ and $k_{trans} \cdot mRNC(i, t)$ were omitted.

The rate constants and other parameters used in the simulation are summarized in Table S1. The elongation rate constant (k_{trans}) was set to 2 residues per second, as reported previously (*15*). k_i^{PDF} and k_i^{MAP} are the pseudo-first-order rate constants for the PDF and MAP reactions at chain length

i, respectively, and were calculated from $(k_{cat}/K_m)^{PDF}$ · [PDF] and $(k_{cat}/K_m)^{MAP}$ · [MAP]. We assumed that NME initiated when the nascent chain length reached 45 residues; hence $(k_{cat}/K_m)^{PDF}$ and $(k_{cat}/K_m)^{MAP}$ were set to zero for nascent chains that are 0-44 amino acids long. Values of $(k_{cat}/K_m)^{PDF}$ and $(k_{cat}/K_m)^{MAP}$ at nascent chain lengths 45, 49, 67, 82, and 127 were experimentally measured, those at in-between nascent chain lengths were linearly interpolated from experimental data, and those for nascent chains longer than 127 residues were set to be the same as for $RNC_{FtsQ127}$. The total concentrations of PDF and MAP were determined to be ~300 nM by quantitative western blot in S30 extract (Fig. S6B, C). We found that the activity of endogenous MAP in the cell extract was ~2 fold lower than that of the recombinant enzyme (Figs. S6E–F); hence, a two-fold correction was made to the absolute MAP concentration to obtain an effective MAP concentration. Depletion of enzyme due to interaction with non-translating ribosome (2.6 μM in S30 extract) was corrected by the same method as in measurements of reactions using purified RNCs (see Eq 4 under "*Kinetic analysis*").

A Matlab script was used to simulate the time-dependent concentration of each species using the numerical integration method. The initial concentrations at t = 0 were set to 1 for *fmRNC* (1,0) and 0 for all other species. A step size of 0.05 s was used to simulate the cotranslational NME of a 300-residue nascent protein (n = 300) over the time-course of 150 s. The time-course was extended to 600 s for the simulations with k_{trans} = 0.5 and 1 s^{-1} in Figs. 4B–E and Figs. S8A–D. To estimate the contribution of experimental errors to the simulation result, the enzyme concentrations, dissociation constants, and the values of k_{cat}/K_m were randomly selected from normal distributions described by the mean value and relative S.D., and the simulation was repeated 100 times.

Supplementary Figures

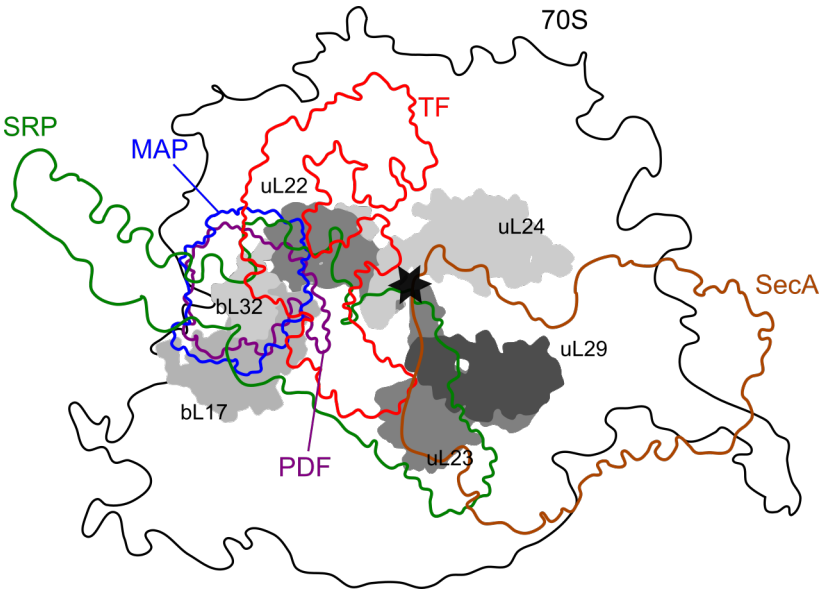

Figure S1: Structure projections of various RPBs on the ribosome.

PDF (purple), MAP (blue), TF (red), SRP (green) and SecA (brown) were shown as outlines of the projections on 70S ribosome from the view of the large subunit, based on reported structures and models (PDB-4V4Q, EMD-9750, EMD-9751, EMD-1499, EMD-1250 and EMD-2564) (*16–19*). Projections of ribosomal proteins near the exit site (star) were indicated.

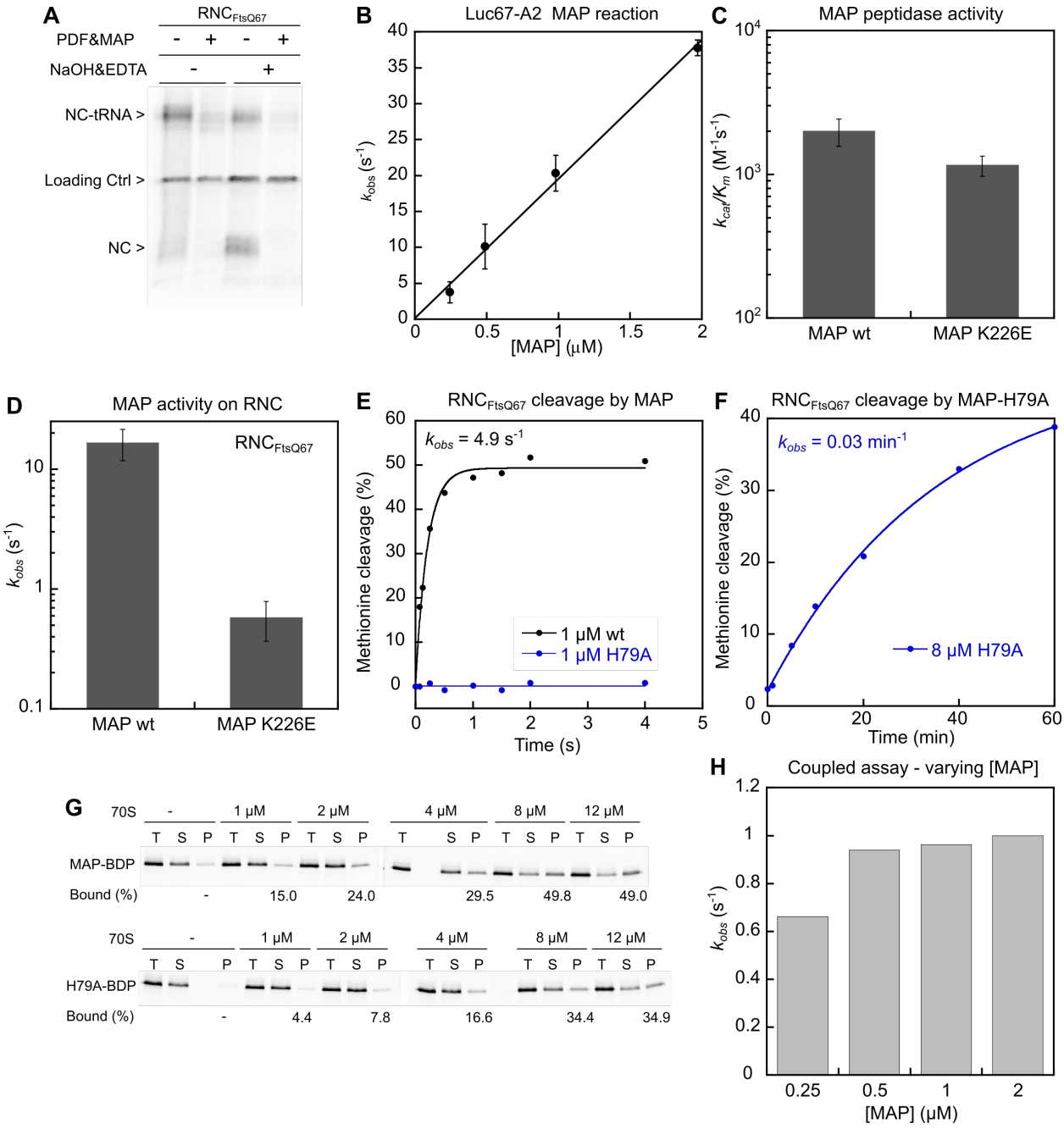

Figure S2: Validations of the assays for MAP and PDF reactions. (A) Autoradiograph of purified RNC$_{FtsQ67}$. The N-terminal methionine on the nascent chain (NC) was ^{35}S-labeled and was cleaved by incubation with 3 μM PDF and MAP ('+' lanes). The NC-tRNA conjugate was verified by hydrolysis with 100 mM NaOH and 25 mM EDTA (42 °C, 30 min) after the reaction (lanes 3 and 4). (B) The MAP concentration dependence of observed rate constants for methionine cleavage of RNC bearing the N-terminal 67 residues of luciferase (Luc). The second residue (Asn)

of luciferase is mutated to alanine such that the N-terminal sequence (MADAK) allows cleavage by PDF and MAP. Linear fit of the data gave a k_{cat}/K_m value of (1.9± 0.06) × 10^7 $M^{-1}s^{-1}$. Data are shown as mean ± S.D., with n = 2. (C) Comparison of the peptidase activities between wildtype MAP and MAP-K226E, using a tetra-peptide (MGMM) as substrate. Data are shown as mean ± S.D., with n = 2. (D) Observed rate constants of wildtype MAP and MAP-K226E for methionine excision on RNC_{FtsQ67}. The reactions were measured as in Fig. 1B with 10 nM RNC_{FtsQ67}, 50 nM PDF, and 1 μM wildtype MAP or MAP-K226E. Data are shown as mean ± S.D., with n = 3. (E) Representative time traces for the cleavage of 10 nM $RNC_{Met\text{-}FtsQ67}$ by 1 μM wildtype MAP (black) or mutant MAP-H79A (blue). (F) The cleavage of $RNC_{Met\text{-}FtsQ67}$ by MAP-H79A (8 μM) was carried out over a longer time course to measure the observed reaction rate constant for this mutant. (G) Representative image for the binding of wildtype MAP and MAP-H79A to 70S ribosome, measured by the co-sedimentation assay. 1 μM BODIPY-labeled MAP or MAP-H79A was incubated with indicated concentrations of 70S ribosomes at room temperature for 20 min in binding buffer (50 mM Hepes-KOH, 50 mM KOAc, 10 mM $Mg(OAc)_2$, 0.1 mM $CoCl_2$, pH 7.5). 40 μL of the reaction was loaded onto 80 μL of 20% sucrose in binding buffer, and centrifuged in TLA100 rotor (Beckman Coulter) at 80,000 rpm, 4 °C for 75 min. The ribosome pellet was resuspended with 40 μL of SDS sample loading dye (50 mM Tris-HCl, 1% SDS, 10% glycerol, 100 mM DTT, pH 6.8). Total reaction (T), supernatant (S) and pellet (P) were analyzed by SDS-PAGE and quantified with Typhoon FLA7000 fluorescence imager. The values underneath are the amount of ribosome-bound MAP, determined by the fluorescence intensities in the pellet lane to the corresponding total lane. (H) The observed rate constant for deformylation of $RNC_{fMet\text{-}FtsQ67}$, measured using the coupled assay in Figure 2B, was determined with 1 μM PDF and indicated concentrations of MAP. The observed rate constant did not change significantly at MAP concentrations above 0.5 μM, indicating that the MAP reaction is not rate-limiting under these conditions.

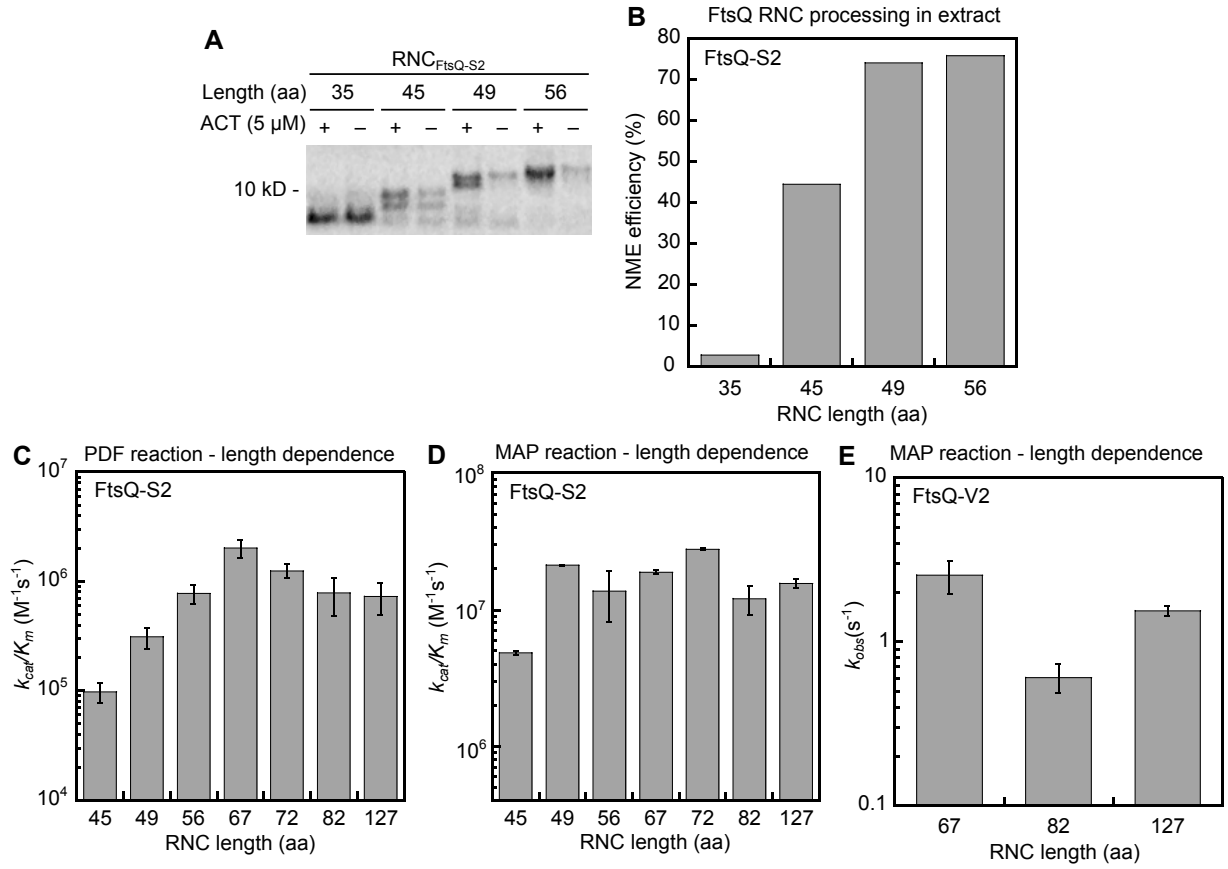

Figure S3: Length dependence of NME reactions. (A) NME of RNC_{FtsQ} with different nascent chain lengths in cell extract. RNCs bearing FtsQ nascent chains containing a single N-terminal ^{35}S-Methionine were generated by *in vitro* translation in the S30 extract and allowed to be processed by endogenous PDF and MAP during a 1-h translation ('– actinonin' lanes). The '+ actinonin' lanes provide controls for the amount of RNC without NME. The extent of NME was analyzed by SDS-PAGE and autoradiography. (B) Quantification of the data in (A) by normalizing the nascent peptide signals in the '– actinonin' lanes relative to parallel translations in the '+ actinonin' lanes. **(**C), (D) Summary of the k_{cat}/K_m values of the PDF (C) and MAP (D) reactions for RNCs bearing FtsQ-S2 nascent chains of the indicated lengths. The PDF reaction rate constants were measured using the coupled deformylation assay (Fig. 2B). (E) Observed rate constants of MAP reactions on $RNC_{FtsQ-V2}$ at the indicated nascent chain lengths. Reactions were measured with 10 nM $RNC_{FtsQ-V2}$ and 1 μM MAP. Values in (C)–(E) are shown as mean ± S.D., with n = 2–3.

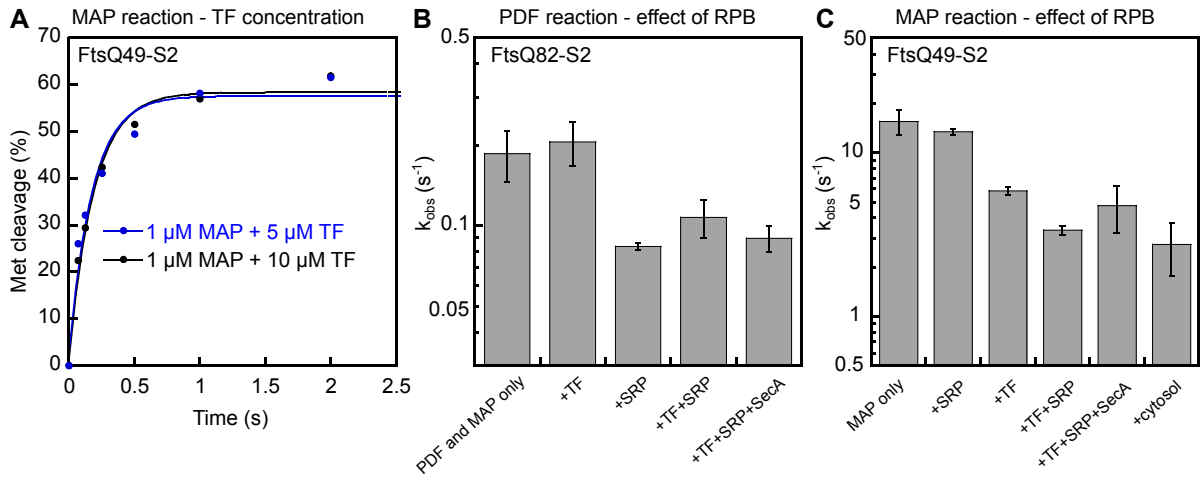

Figure S4: RPB effects on NME reactions. (A) Time traces for cleavage of 10 nM $RNC_{FtsQ49\text{-}S2}$ by 1 μM MAP in the presence of 5 μM (blue) or 10 μM (black) TF. The data were fit to Eq. 1 and gave k_{obs} values of 5.6 and 5.3 s^{-1}, respectively, indicating the saturation of TF effect on the MAP reaction. (B) Effects of TF, SRP and SecA on the deformylation of $RNC_{FtsQ49\text{-}S2}$. Observed rate constants were measured with 10 nM $RNC_{FtsQ82\text{-}S2}$, 0.5 μM PDF and 1 μM MAP using the coupled assay. Where indicated, the reactions also contained 5 μM TF, 400 nM SRP, and 1 μM SecA. (C) Effects of TF, SRP, SecA, or ribosome-free cytosol on methionine cleavage of $RNC_{FtsQ49\text{-}S2}$ by MAP. Observed rate constants were measured with 10 nM $RNC_{FtsQ49\text{-}S2}$ and 1 μM MAP. The '+cytosol' reaction contained 28% (v/v) of ribosome-free S30 extract with ~110 nM endogenous MAP (see Materials and Methods and Fig. S6D). The data in (B) and (C) are shown as mean ± S.D., with n = 2.

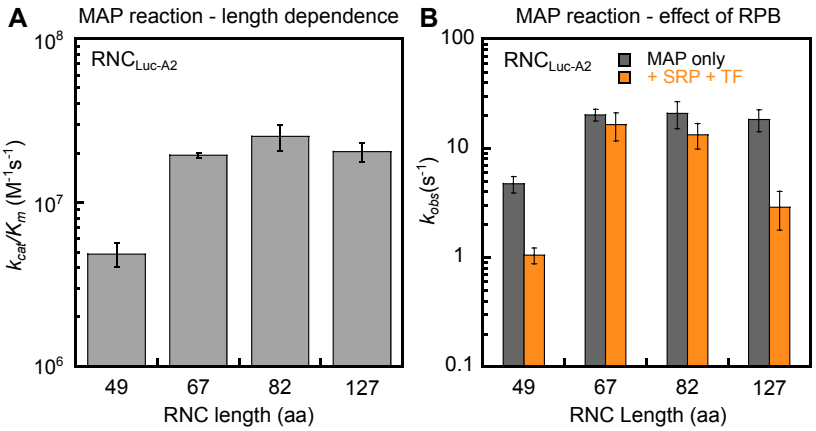

Figure S5: Length dependence and RPB effect on MAP reactions of RNC$_{Luc.}$ (A) Summary of the k_{cat}/K_m values of the MAP reaction for RNCs bearing the luciferase nascent chain of indicated lengths. (B) Effects of TF and SRP on methionine cleavage of RNCs bearing the luciferase nascent chains of indicated lengths. Observed rate constants were measured with 10 nM RNCs and 1 μM MAP. All data are shown as mean ± S.D., with n = 2.

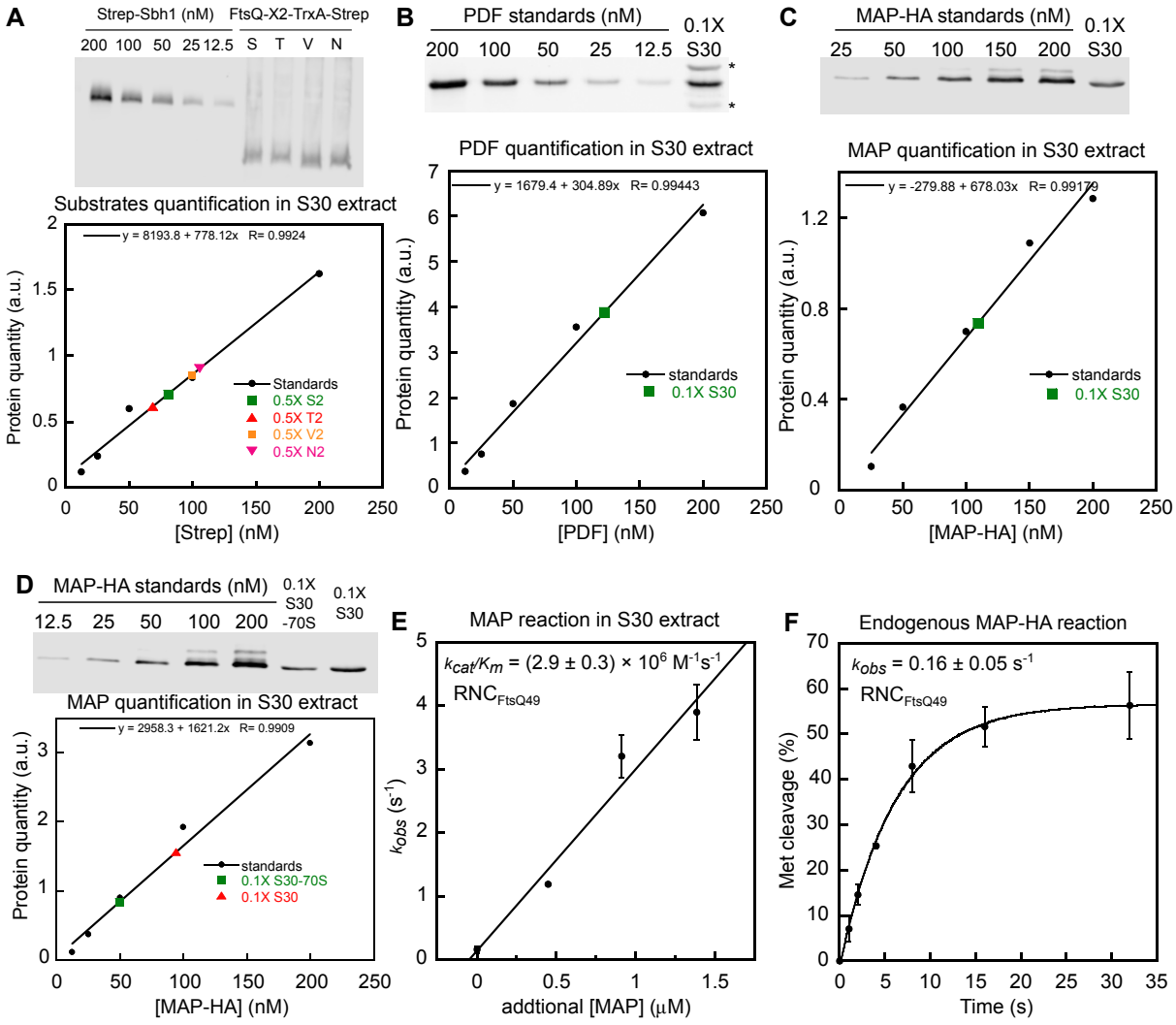

Figure S6: Characterization of endogenous PDF and MAP-HA in cell extracts (A) Anti-Strep immunoblot (upper panel) to measure the concentrations of the substrates for the cotranslational NME assay, FtsQ-X2-TrxA-Strep, translated for 30 min at 30 °C in S30 extract. Known concentrations of a purified Strep-tagged protein, Sbh1, were used to construct a standard curve for the quantification (lower panel, black line). The substrate concentrations were determined to be 150–200 nM; as ribosomes were being turned over during translation, these values are upper limits of the substrate concentration during cotranslational NME. (B) A representative anti-PDF immunoblot (upper panel) to measure the endogenous level of PDF in S30 extract. Known concentrations of purified PDF were used to construct a standard curve for quantification (lower panel). The PDF concentration was determined to be 320 ± 20 nM (S.D., n = 3) in the *in-vitro* translation (IVT) reactions, which contained 28% (v/v) of S30 extract. The asterisks denoted non-

specific bands. (C) Representative western blot (upper panel) to determine the endogenous level of MAP in S30 extract. To facilitate quantification, an HA tag was engineered C-terminal to the genomic MAP. The activity of MAP-HA in the cell extract was comparable to that of wild-type MAP (Fig. S9). Known concentrations of purified MAP-HA were used to construct a standard curve for the quantification (lower panel). The concentration of MAP-HA was determined to be 250 ± 50 nM (S.D., n = 4) under IVT conditions. (D) A representative anti-HA immunoblot to measure the endogenous level of MAP-HA in S30 extract and in ribosome-free cytosol (S30–70S) used in the reactions shown in Figures S6E, S6F, and S4C. The concentration of MAP-HA in the ribosome-free extract was determined to be 110 ± 40 nM (S.D., n = 2) under IVT conditions. (E) Observed rate constants for methionine cleavage of $RNC_{FtsQ49\text{-}S2}$ in the presence of ribosome-free cytosol were plotted as a function of MAP concentration. The reactions contained 10 nM RNC, 28% (v/v) ribosome-free S30 extract with ~110 nM endogenous MAP (measured in (D)), and indicated concentrations of purified MAP. The line is a linear fit of the data, and the obtained k_{cat}/K_m value is indicated. (F) Time course for methionine cleavage of $RNC_{FtsQ49\text{-}S2}$ by endogenous MAP-HA in the S30 extract. The reaction contained 10 nM RNC and 28% (v/v) ribosome-free S30 extract containing ~110 nM endogenous MAP. The data were fit to single exponential function and gave a k_{obs} value of 0.16 ± 0.05 s^{-1}, ~2-fold slower than that expected based on the k_{cat}/K_m value measured in Fig. S6E, suggesting that endogenous MAP has 2-fold lower activity than purified MAP. Values in (E) and (F) are shown as mean ± S.D., with n = 2.

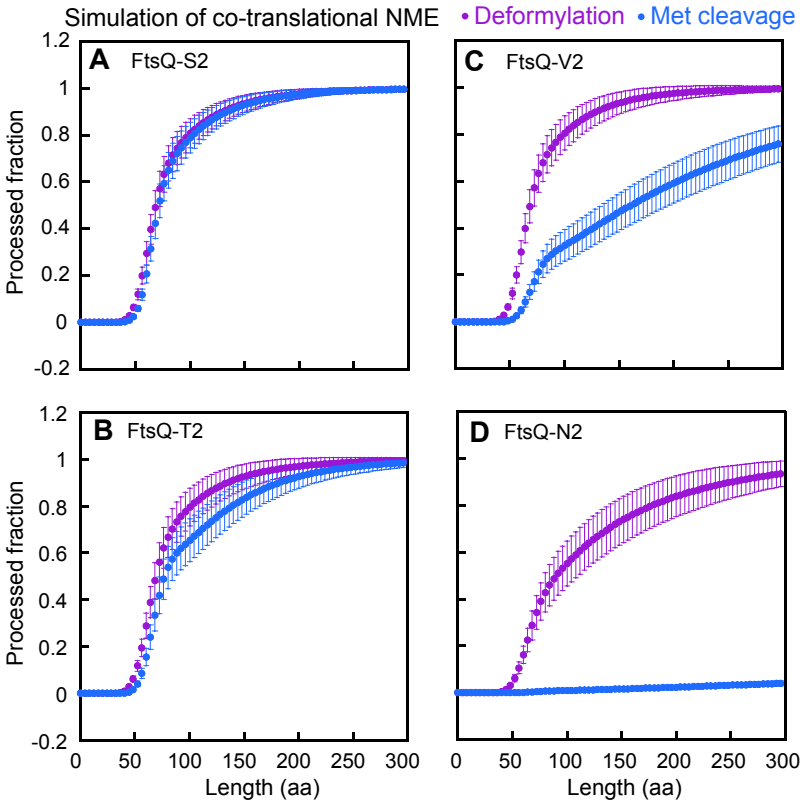

Figure S7: Comparison of the simulated reaction profiles for cotranslational deformylation (magenta) and methionine cleavage (blue) of FtsQ-X2 in the presence of RPBs. The profiles were plotted as the cumulative fraction of processed RNCs over time, which was converted to the nascent chain length being synthesized. For each independent run, the enzyme concentrations and the processing rates were randomly selected from normal distributions with a relative S.D. of 20%. Results from 100 runs were shown as mean ± S.D.

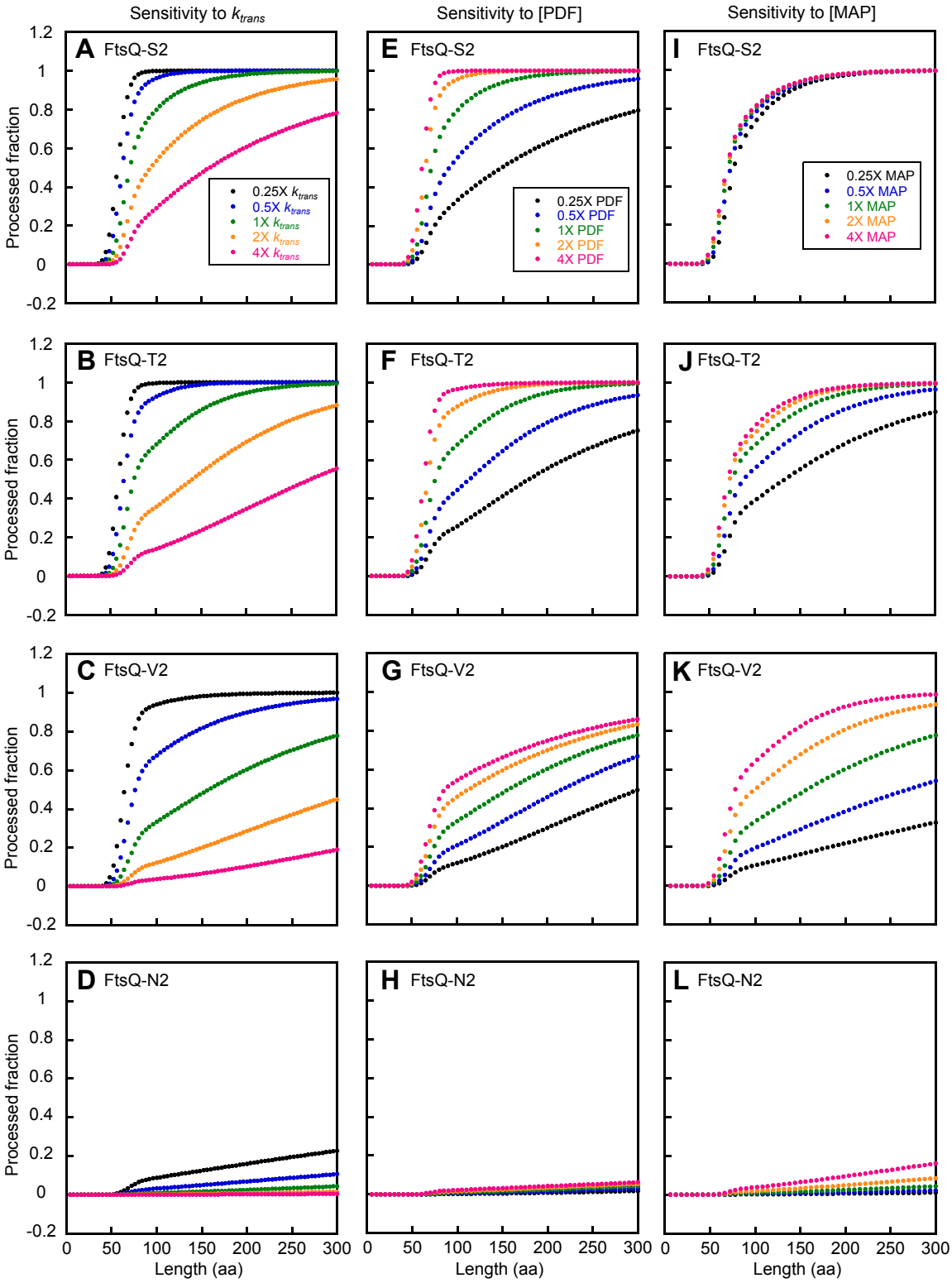

Figure S8: The individual NME reaction profiles generated during the sensitivity test shown in Figs. 4B–E.

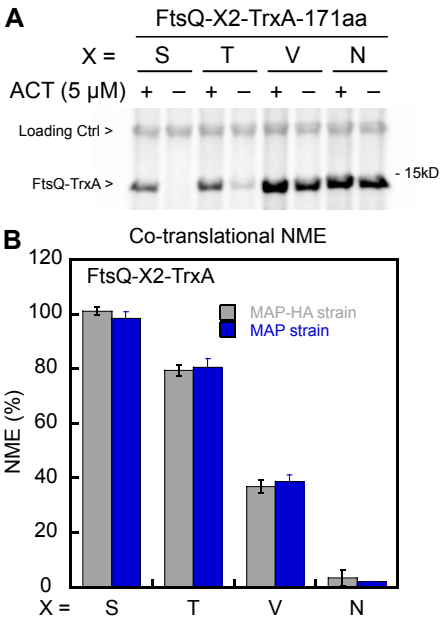

Figure S9: The C-terminal HA tag did not affect MAP function. (A) Representative SDS-PAGE and autoradiography analysis of cotranslational processing of FtsQ-X2-TrxA in the S30 extract prepared from *E. coli* strain harboring MAP-HA. (B) Quantification of the cotranslational NME efficiency from the data in (A) and replicates, and comparison with the NME efficiency from the S30 extract from the wild-type strain (Fig. 5D).

Table S1: Parameters used in the kinetic simulation model. All values are represented as mean ± S.D., and the relative S.D. are indicated in parentheses. The RPB effect is represented as folds decrease relative to the condition without RPBs. The effects of second residues and nascent chain length for T2, V2, N2 are represented as folds reduction relative to S2.

ribosome	2.6 ± 0.3 μM (10%)	Free [PDF] = 130 ± 25 nM (20%) Free [MAP] = 63 ± 15 nM (20%)
[PDF]	320 ± 20 nM (10%)	
[MAP]	130 ± 25 nM (20%)	
K_d^{PDF}	1.8 ± 0.5 μM (30%)	
K_d^{MAP}	2.4 ± 0.4 μM (20%)	
k_{trans}	2 aa/s	

k_{PDF} (20%)	Length	45	49	56	67	72	82	127
	k_{cat}/K_m (10^6 $M^{-1}s^{-1}$)	0.098	0.31	0.76	2.0	1.3	0.78	0.73
	RPB effect	2						
	Second residue effect	S2: 1 T2: 1 V2: 1 N2: 2						

k_{MAP} (20%)	Length	45	49	56	67	72	82	127
	k_{cat}/K_m (10^7 $M^{-1}s^{-1}$)	0.14	2.1	1.4	1.9	2.8	1.2	1.6
	RPB effect for S2	4.6	4.6	3.2	1.1	1.1	1.3	1.7
	RPB effects for T2, V2, N2	2.4	2.4	2	1.6	2	3	8
	Length effects for T2, V2, N2	3.6	3.6	1	1	1	2	1
	Second residue effect	S2: 1 T2: 2 V2: 10.3 N2: 294						

Supplementary References

1. D. G. Gibson, L. Young, R.-Y. Chuang, J. C. Venter, C. A. Hutchison, H. O. Smith, Enzymatic assembly of DNA molecules up to several hundred kilobases. *Nat. Methods*. **6**, 343–345 (2009).

2. J. Norrander, T. Kempe, J. Messing, Construction of improved M13 vectors using oligodeoxynucleotide-directed mutagenesis. *Gene*. **26**, 101–106 (1983).

3. C. Schaffitzel, N. Ban, Generation of ribosome nascent chain complexes for structural and functional studies. *J Struct Biol*. **158**, 463–71 (2007).

4. C. Li, A. Wen, B. Shen, J. Lu, Y. Huang, Y. Chang, FastCloning: a highly simplified, purification-free, sequence- and ligation-independent PCR cloning method. *BMC Biotechnol.* **11**, 92 (2011).

5. M. C. Jewett, J. R. Swartz, Mimicking the Escherichia coli cytoplasmic environment activates long-lived and efficient cell-free protein synthesis. *Biotechnol. Bioeng.* **86**, 19–26 (2004).

6. K. A. Calhoun, J. R. Swartz, Total amino acid stabilization during cell-free protein synthesis reactions. *J Biotechnol*. **123**, 193–203 (2006).

7. K. A. Datsenko, B. L. Wanner, One-step inactivation of chromosomal genes in Escherichia coli K-12 using PCR products. *Proc. Natl. Acad. Sci. U.S.A.* **97**, 6640–6645 (2000).

8. S. Ragusa, S. Blanquet, T. Meinnel, Control of peptide deformylase activity by metal cations. *J. Mol. Biol.* **280**, 515–23 (1998).

9. F. Frottin, A. Martinez, P. Peynot, S. Mitra, R. C. Holz, C. Giglione, T. Meinnel, The proteomics of N-terminal methionine cleavage. *Mol. Cell Proteomics*. **5**, 2336–49 (2006).

10. I. Saraogi, D. Zhang, S. Chandrasekaran, S. O. Shan, Site-specific fluorescent labeling of nascent proteins on the translating ribosome. *J. Am. Chem. Soc.* **133**, 14936–9 (2011).

11. W. W. Cleland, Partition analysis and concept of net rate constants as tools in enzyme kinetics. *Biochemistry*. **14**, 3220–3224 (1975).

12. A. Sandikci, F. Gloge, M. Martinez, M. P. Mayer, R. Wade, B. Bukau, G. Kramer, Dynamic enzyme docking to the ribosome coordinates N-terminal processing with polypeptide folding. *Nat. Struct. Mol. Biol.* **20**, 843–50 (2013).

13. R. Bingel-Erlenmeyer, R. Kohler, G. Kramer, A. Sandikci, S. Antolic, T. Maier, C. Schaffitzel, B. Wiedmann, B. Bukau, N. Ban, A peptide deformylase-ribosome complex reveals mechanism of nascent chain processing. *Nature*. **452**, 108–11 (2008).

14. C. P. Guimaraes, M. D. Witte, C. S. Theile, G. Bozkurt, L. Kundrat, A. E. Blom, H. L. Ploegh, Site-specific C-terminal internal loop labeling of proteins using sortase-mediated reactions. *Nat Protoc*. **8**, 1787–99 (2013).

15. K. A. Underwood, J. R. Swartz, J. D. Puglisi, Quantitative polysome analysis identifies limitations in bacterial cell-free protein synthesis. *Biotechnol. Bioeng.* **91**, 425–435 (2005).

16. B. S. Schuwirth, M. A. Borovinskaya, C. W. Hau, W. Zhang, A. Vila-Sanjurjo, J. M. Holton, J. H. D. Cate, Structures of the Bacterial Ribosome at 3.5 Å Resolution. *Science*. **310**, 827–834 (2005).

17. S. Bhakta, S. Akbar, J. Sengupta, Cryo-EM Structures Reveal Relocalization of MetAP in the Presence of Other Protein Biogenesis Factors at the Ribosomal Tunnel Exit. *J. Mol. Biol.* **431**, 1426–1439 (2019).

18. F. Merz, D. Boehringer, C. Schaffitzel, S. Preissler, A. Hoffmann, T. Maier, A. Rutkowska, J. Lozza, N. Ban, B. Bukau, E. Deuerling, Molecular mechanism and structure of Trigger Factor bound to the translating ribosome. *EMBO J.* **27**, 1622–1632 (2008).

19. C. Schaffitzel, M. Oswald, I. Berger, T. Ishikawa, J. P. Abrahams, H. K. Koerten, R. I. Koning, N. Ban, Structure of the E. coli signal recognition particle bound to a translating ribosome. *Nature*. **444**, 503–6 (2006).